

The orbital period of the recurrent nova V2487 Oph revealed

Pablo Rodríguez-Gil^{1,2*}, Jesús M. Corral-Santana³, N. Elías-Rosa^{4,5}, Boris T. Gänsicke⁶,
Margarita Hernanz^{5,7} and Gloria Sala^{8,7}

¹*Instituto de Astrofísica de Canarias, E-38205 La Laguna, Tenerife, Spain*

²*Departamento de Astrofísica, Universidad de La Laguna, E-38206 La Laguna, Tenerife, Spain*

³*European Southern Observatory, Alonso de Córdova 2107, Vitacura, Casilla 19001, Santiago de Chile, Chile*

⁴*INAF – Osservatorio Astronomico di Padova, Vicolo dell’Osservatorio 5, 35122, Padova, Italy*

⁵*Institute of Space Sciences (ICE, CSIC), Campus UAB, Camí de Can Magrans s/n, 08193, Barcelona, Spain*

⁶*Department of Physics, University of Warwick, Coventry CV4 7AL, UK*

⁷*Institut d’Estudis Espacials de Catalunya (IEEC), Barcelona, Spain*

⁸*Departament de Física EEBE, Universitat Politècnica de Catalunya (UPC), Barcelona, Spain*

Accepted 2023. Received 2023; in original form 2023

ABSTRACT

We present the first reliable determination of the orbital period of the recurrent nova V2487 Oph (Nova Oph 1998). We derived a value of 0.753 ± 0.016 d (18.1 ± 0.4 h) from the radial velocity curve of the intense He II $\lambda 4686$ emission line as detected in time-series X-shooter spectra. The orbital period is significantly shorter than earlier claims, but it makes V2487 Oph one of the longest period cataclysmic variables known. The spectrum of V2487 Oph is prolific in broad Balmer absorptions that resemble a white dwarf spectrum. However, we show that they come from the accretion disc viewed at low inclination. Although highly speculative, the analysis of the radial velocity curves provides a binary mass ratio $q \approx 0.16$ and a donor star mass $M_2 \approx 0.21 M_\odot$, assuming the reported white dwarf mass $M_1 = 1.35 M_\odot$. A subgiant M-type star is tentatively suggested as the donor star. We were lucky to inadvertently take some of the spectra when V2487 Oph was in a flare state. During the flare, we detected high-velocity emission in the Balmer and He II $\lambda 4686$ lines exceeding -2000 km s⁻¹ at close to orbital phase 0.4. Receding emission up to 1200 km s⁻¹ at about phase 0.3 is also observed. The similarities with the magnetic cataclysmic variables may point to magnetic accretion on to the white dwarf during the repeating flares.

Key words: accretion, accretion discs – binaries: close – novae, cataclysmic variables – stars: individual: V2487 Oph (Nova Ophiuchi 1998)

1 INTRODUCTION

The orbital period of the Galactic nova V2487 Oph (Nova Ophiuchi 1998) has eluded detection until now. This is certainly not because of any known inherent difficulties of observation, but rather because V2487 Oph remains insufficiently explored.

The analysis of the X-ray spectrum reported in [Hernanz & Sala \(2002\)](#) pointed to a magnetic white dwarf in the binary, with the spectrum resembling those observed in cataclysmic variables (CVs) of the intermediate polar class. In addition, they found a rather high plasma temperature (≥ 48 keV) in the hard X-ray spectrum, which suggests accretion onto a massive white dwarf.

After the 1998 nova event ([Nakano et al. 1998](#)), the suggestion of [Hachisu et al. \(2002\)](#) that the object is a recurrent nova and the finding of a preceding eruption in 1900 by [Pagnotta et al. \(2009\)](#) using Harvard College Observatory photographic plates placed this very fast nova ($t_3 = 8$ d, with t_3 the time to decline by 3 mag from the nova peak brightness) in the limelight again (see [Schaefer 2010](#), for more details). [Schaefer, Pagnotta & Zoppelt \(2022\)](#) communicated the finding of "superflares" in *K2* data obtained in 2009. These are

observed to recur daily and have a duration of about one hour, which they attributed to the reconnection of accretion disc magnetic field lines after being twisted and amplified due to the disc motion, in a similar way as in the Sun and flare stars.

Under the assumption that V2487 Oph is a member of the U Sco subclass, an orbital period of about one day was suggested ([Hachisu et al. 2002](#); [Schaefer 2010](#)). In this paper, we report on VLT/X-shooter time-series spectroscopy of V2487 Oph that allowed us to measure its orbital period. Section 2 deals with the spectroscopic data and their reduction. Section 3 describes the average spectrum of V2487 Oph and provides a list of the most prominent spectral lines. In Section 4, we present and describe our results, and give our conclusions in Section 5.

2 OBSERVING DATA

We collected spectra of V2487 Oph over the nights of 2019 June 7, 8 and 9 with the X-shooter échelle spectrograph ([Vernet et al. 2011](#)) mounted on UT2 at the 8.2-m VLT in Cerro Paranal, Chile. A total of 210 spectra in nodding mode following the usual ABBA pattern were obtained per spectrograph arm with a nodding throw of 4 arcsec. On every night, we used a repeating observing sequence that

* E-mail: prguez@iac.es (PRG)

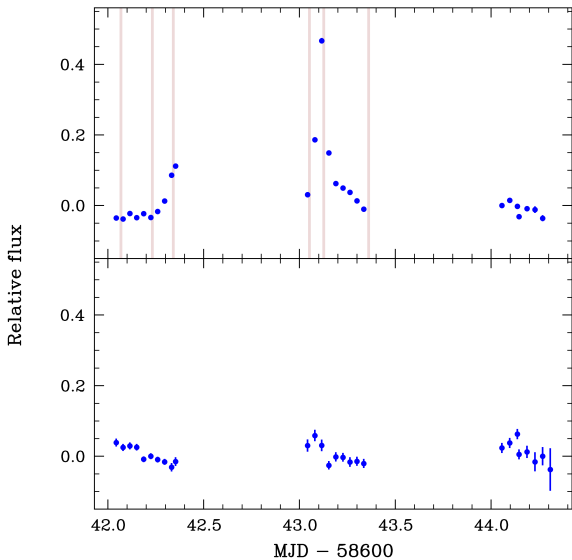


Figure 1. Top panel: light curve of V2487 Oph relative to a nearby comparison star derived using the X-shooter acquisition images for the three observing nights (2019 June 7, 8 and 9). A flare is detected at the beginning of the second night, while the onset of a flare may have been detected on the first night. The vertical lines mark the central times of the spectra shown in Fig. 8. Bottom panel: light curve of the comparison star used for V2487 Oph relative to a check star. The median flux of the whole data set has been subtracted in both panels for display purposes.

starts with an acquisition image followed by two ABBA nod cycles. The slit widths were 1.0, 0.9 and 0.9 arcsec for the ultraviolet-blue (UVB), visible (VIS) and near-infrared (NIR) arms, respectively, which provided approximate central spectral resolutions of 55, 34 and 53 km s^{-1} . We used integration times of 300, 312 and 315 s on the first two nights, that were increased by 50 s on the last night due to cloud patches. The spectral data were reduced with version v2.8.5 of the ESO REFLEX pipeline. Every individual spectrum used in the analysis presented below is the average of an ABBA cycle except for a few spectra coming from AB blocks at the end of the nightly allocated observing time.

2.1 The X-shooter acquisition image light curve

To check if any of our spectra were obtained by chance during a "superflare" of V2487 Oph (hereinafter flare), we first checked whether our X-shooter spectroscopy was unintentionally covered by any of Schaefer et al. (2022)'s light curves in which they detected flares. Unfortunately, the X-shooter spectra lie outside their time baseline. However, as explained in Section 2, our observing strategy always started with an acquisition image, followed in general by two ABBA nod cycles. In order to check for flares in the acquisition images, we carried out variable aperture photometry of V2487 Oph and a comparison and a check star nearby with the HiPERCAM pipeline¹. The resulting light curves, shown in Fig. 1, clearly show a flare on the second night and, possibly, the onset of another one on the first night.

¹ <https://cygnus.astro.warwick.ac.uk/phsaap/hipercam/docs/html/>

3 THE X-SHOOTER SPECTRUM OF V2487 Oph

For the interstellar reddening correction we adopted a colour excess $E(B - V) = 0.6$, calculated using the 3D interstellar dust map of Green et al. (2019)² and the distance $d = 6.4 \pm 1.6 \text{ kpc}$ derived by Bailer-Jones et al. (2021) from the *Gaia* eDR3 parallax.

The unreddened average spectra (0.3080 to $2.4800 \mu\text{m}$) are presented in Fig. 2. We illustrate in red the average of the spectra in quiescence, while in blue we plot the average of the spectra taken during a flare (i.e. the average of all the spectra acquired on the second night).

The spectrum of V2487 Oph displays a hot continuum consistent with the photometric spectral energy distribution presented in Schaefer et al. (2022), which suggests a dominant contribution of the accretion disc. However, the H I and some He I emission lines are blended with much broader absorptions. At face value, these absorption lines might resemble those of a hot white dwarf. Adopting a white dwarf mass $M_{\text{WD}} = 1.35 M_{\odot}$ (Hachisu et al. 2002), $T_{\text{eff}} = 80\,000 \text{ K}$, and $d = 6.4 \text{ kpc}$, the apparent magnitude of the white dwarf is ≈ 25 , i.e. any contribution of a white dwarf to the observed optical flux of V2487 Oph is negligible. This supports the conclusion that the Balmer absorption lines originate in the accretion disc. In fact, as we will see in Section 4.1, the phasing of the absorption-line radial velocity curves confirms this.

The X-shooter spectrum of V2487 Oph also reveals several He II emission lines, with the Fowler series He II $\lambda 4686$ line the strongest, exceeding H β in intensity. Remarkably, the spectrum shows a number of double-ionised oxygen emission lines, that are direct evidence for the Bowen fluorescence mechanism (Bowen 1934). The O III fluorescence lines involve trapping of He II Ly α $\lambda 303.782$ photons by the O III $2p^2 \text{ } ^3\text{P}_2 - 2p3d \text{ } ^3\text{P}_2$ transition at 303.799 \AA , followed by cascade transitions (see e.g. McClintock, Canizares & Tarter (1975); Schachter et al. 1991). Primary cascade O III $\lambda\lambda 3133, 3429, 3444$ (O1 channel) and secondary cascade O III $\lambda\lambda 3299, 3312, 3341$ emissions are clearly detected in the UVB-arm spectrum of V2487 Oph, as is the O III $\lambda 3122$ fluorescence line as a result of excitation of the $2p3d \text{ } ^3\text{P}_1$ level by He II Ly α $\lambda 303.70$ photons (O3 channel). The C III/N III $\lambda\lambda 4634-4651$ Bowen fluorescence blend is also observed.

As we will later show, the radial velocity curves of the broad component in the most intense O III emissions at 3133 and 3444 \AA indicate an origin on the white dwarf side of the binary system (Fig. 11). However, the narrow component follows the motion of the companion star. O III fluorescence emission lines have also been reported in some strongly-magnetic CVs, known as polars. Examples are AM Her, the precursor of the class (Raymond et al. 1979; Schachter et al. 1991), EF Eri (Schachter et al. 1991), and RX J1802.1+1804 (Shrader, Singh & Barrett 1997). In Table 1 we list the wavelengths of the most prominent lines identified in the X-shooter spectrum of V2487 Oph.

4 RESULTS

4.1 The orbital period

We conducted a period search on the He II $\lambda 4686$ emission line radial velocity curve, that was derived by cross-correlating the line profile in the average spectrum of every ABBA set with a FWHM = 300 km s^{-1} Gaussian template. Prior to this, the adjacent continuum

² <http://argonaut.skymaps.info>

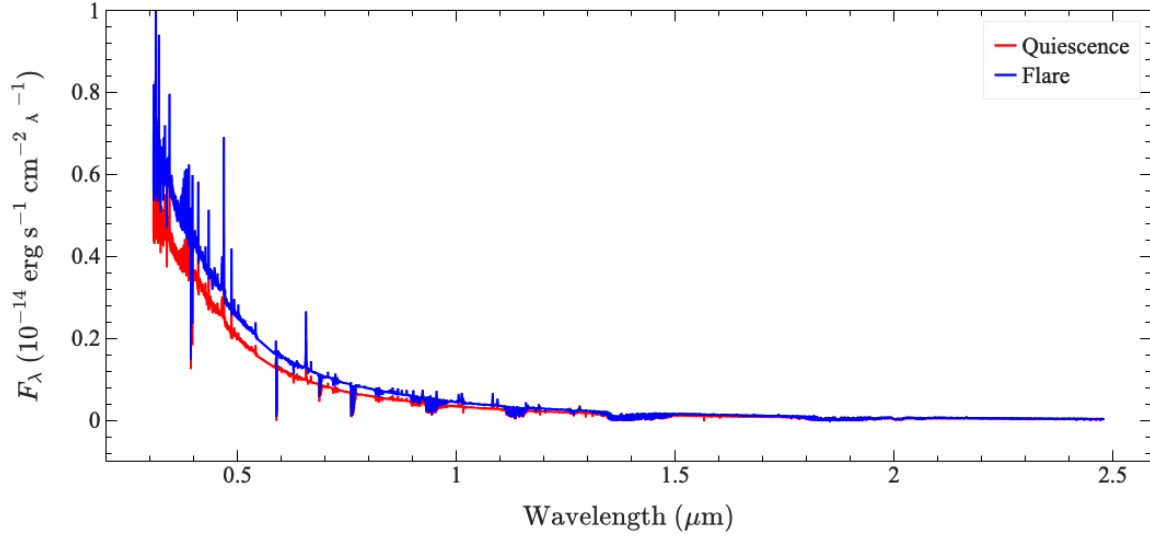


Figure 2. X-shooter average spectra of V2487 Oph in quiescence (red) and during a flare (blue). The fluxes were corrected for interstellar reddening using $E(B - V) = 0.6$. An online interactive version of this plot is available. Left-mouse-click on the legend label in the online plot to hide/show the sibling data set.

Table 1. Most prominent emission lines observed in the X-shooter average spectrum of V2487 Oph. Fluorescent lines are abbreviated as “fluo.”

Line	λ (μm)	Line	λ (μm)	Line	λ (μm)
O III	0.3122	He I	0.4026	Mg II	0.7896
O III	0.3133 fluo.	O III + C III	0.4071	O I	0.8446
He II	0.3203	H δ	0.4102	Pa17	0.8467
O III	0.3265	He I	0.4121	Ca II + Pa16	0.8498
O III	0.3299 fluo.	C II	0.4267	Ca II + Pa15	0.8542
O III	0.3312 fluo.	H γ	0.4340	Pa14	0.8598
O III	0.3341 fluo.	He I	0.4388	Ca II + Pa13	0.8662
O III	0.3429 fluo.	He I	0.4472	Pa12	0.8750
O III	0.3444 fluo.	Mg II	0.4481	Mg I?	0.8807
He I	0.3587	C III/N III fluo.	Bowen	Pa11	0.8863
H18	0.3692	He II	0.4686	Pa10	0.9015
H17	0.3697	He I	0.4713	Pa9	0.9229
H16	0.3704	H β	0.4861	Pa ϵ	0.9546
H15	0.3712	He I	0.4922	Pa δ	1.0049
H14	0.3722	He I	0.5016	He II	1.0124
H13	0.3734	He II	0.5412	He I	1.0830
O III	0.3760	He I	0.5876	Pa γ	1.0938
H12	0.3750	H α	0.6563	He II	1.1626
H11	0.3771	C II	0.6578	Pa β	1.2818
H10	0.3798	C II	0.6583	Br14	1.5880
He I	0.3820	He I	0.6678	Br12	1.6406
H9	0.3835	He I	0.7065	Br11	1.6806
H8	0.3889	He I	0.7281	He I	1.7002
Ca II	0.3934	O I	0.7774	Br10	1.7361
He	0.3970	Mg II	0.7877	Br γ	2.1660

was normalised to unity and the spectra were re-binned into a uniform velocity scale.

We subjected the resulting radial velocity curve (bottom panel of Fig. 3) to a generalised Lomb-Scargle analysis (GLS; Zechmeister & Kürster 2009), that uses a constant and a sine wave as the fitting

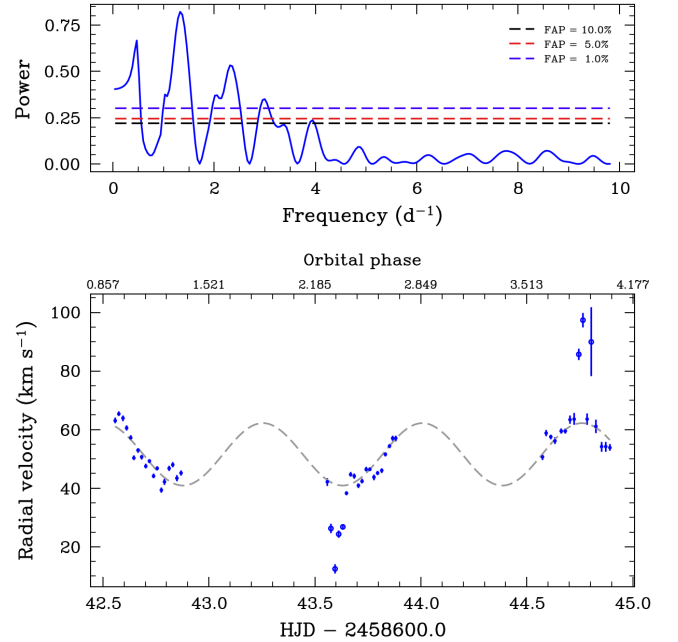


Figure 3. Top panel: Generalized Lomb-Scargle periodogram of the He II $\lambda 4686$ radial velocity curve shown in the bottom panel. The horizontal dashed lines are the 10, 5, and 1 per cent false-alarm probability (FAP) levels. The highest peak provides a period of 0.753 ± 0.016 d (18.1 ± 0.4 h). Bottom panel: radial velocity curve of the He II $\lambda 4686$ emission line. We used a single Gaussian function with $\text{FWHM} = 300$ km s^{-1} as the cross-correlation template. Deviant points are marked as open circles and have been omitted from the period analysis and sinusoid fit (dashed line). The top x-axis shows the orbital phase computed using $T_0(\text{HJD}) = 2458642.6076$.

function. We used the GLS class from PYASTRONOMY³ (Czesla et al. 2019). The periodogram is illustrated in Fig. 3 (top panel). We also calculated the 10, 5, and 1 per cent false-alarm probability (FAP)

³ <https://github.com/sczesla/PyAstronomy>

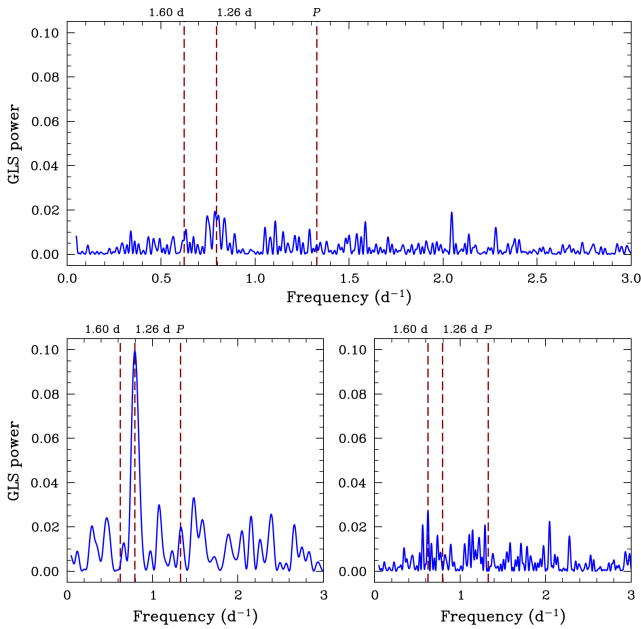


Figure 4. GLS periodograms of the V2487 Oph *K2* light curve (data from table 3 in Schaefer et al. 2022). Top panel: periodogram using the whole *K2* data set. Bottom left panel: same as the top panel, but using the first chunk of the *K2* light curve (26-d time baseline). Bottom right panel: same as the top panel, but using the second chunk of the light curve (15-d time baseline). P is the orbital period derived in this paper from the He II $\lambda 4686$ emission-line radial velocity curve (Section 4.1). Note that the three plots share the same y-axis.

levels in the frequency range shown. They should be interpreted as the probability that at least one out of all the independent power values in that range computed from a white Gaussian noise time series is as large or larger than a given periodogram power threshold.

A period of 0.753 ± 0.016 d ($= 18.1 \pm 0.4$ h) is favoured, which we interpret as the orbital period of V2487 Oph.

4.2 The *K2* photometry revisited

Schaefer et al. (2022) reported a tentative 1.24 ± 0.02 d orbital period based on a Lomb-Scargle periodogram of their approximately 70-d long, 59-s integration *K2* light curve from 2009 data. However, our value is about 40 per cent shorter. For this reason, we conducted a new period search on these *K2* data, that they provide in their table 3. The results are presented in Fig. 4. Both a GLS periodogram and a conditional entropy (CE; not shown) periodogram (Graham et al. 2013) of the whole data set favour a 1.26-d periodicity. However, the periodograms seem to be dominated by the recurrence time scale of the flares in the first *K2* light curve chunk, as illustrated by our periodogram computed from the first 26-d portion of the light curve. The GLS and CE periodograms calculated from the second chunk of the light curve only (15 d) suggest a different periodicity of 1.6 d, with little signal found at 1.26 d. Likewise, the 1.6-d signal is absent in the first chunk. In addition, there is no sign of the orbital period derived by us. This points to a variable flare recurrence time scale in V2487 Oph and makes a direct association with the orbital period or any clock in the system highly unlikely.

4.3 Quiescence and flare trailed spectra diagrams

As described in Section 2.1 (see also Fig. 1), we covered a flare of the system on the second observing night. In order to test for changes between the quiescent and flare spectra with the orbital phase, we used the derived orbital period and the time of inferior conjunction of the companion star (T_0 , calculated in Section 4.4) to assemble the trailed spectrograms that we present in Figs. 5, 6, and 7. Despite the incomplete orbit coverage, there are evident differences.

The H α emission line is exemplary of the behaviour of the Balmer series emission. The trailed spectra during the flare (second night) show a FWHM ≈ 280 km s $^{-1}$ S-wave component with a maximum approaching radial velocity of ≈ -1000 km s $^{-1}$ at about orbital phase $\varphi \approx 0.4$. In addition, H α displays extra emission that extends to a very high approaching velocity, exceeding -2000 km s $^{-1}$, and is only visible in the close vicinity of $\varphi = 0.4$. High-velocity receding emission up to 1200 km s $^{-1}$ is also observed at $\varphi \approx 0.3$. Resemblant high-velocity emission is detected in He II $\lambda 4686$ as well (see Fig. 6), which also appears to show the extra emission peaking at ≈ -2000 km s $^{-1}$ and probably the red counterpart.

The spectra from the second night cover the orbital phase range $\varphi = 0.26 - 0.69$, and the flare peak is observed at $\varphi = 0.35$ on that night. A curve of the normalized flux computed in the velocity range ($-2500, -1200$) km s $^{-1}$ relative to H α (not shown) reaches its maximum at $\varphi = 0.38$, which is consistent with the high-velocity emission being related to the flare.

In Fig. 8 we illustrate the observed line profile changes with the target brightness in selected spectral regions that contain Balmer and He I lines, and the He II $\lambda 4686$ and Bowen blend emissions. The left and right panels of Fig. 8 correspond to the first and second nights, respectively, and time runs from bottom to top.

On the first night, the H β , H γ and H δ broad absorptions originating in the accretion disc are noticeable in the first two spectra displayed ($\varphi = 0.95, 0.17$). However, they are filled up in the third one ($\varphi = 0.32$), which was obtained when V2487 Oph was at its brightest in our observing window, after what may be the onset of a flare. The same happens on the second night, with the accretion disc absorption lines only visible when the system was returning to quiescence after the flare ($\varphi = 0.67$ spectrum).

The changes in the emission line profiles are even more pronounced on the second night, when a flare peak was observed. At $\varphi = 0.36$, H α and He II $\lambda 4686$ display broad emission wings that reflect the presence of the high-velocity S-wave reaching its maximum blue-shift. This is also visible, albeit to a lesser extent, in H β and H γ (see also Fig. A2). The He II $\lambda 4686$ and Bowen blend emissions are at their peaks at this orbital phase.

Schaefer et al. (2022) explained the flares in V2487 Oph as driven by reconnection of magnetic field lines above the accretion disc in a similar manner as in ordinary flare stars. However, it is unclear how this can be reconciled with our detection of high-velocity emission in the emission lines, that bears resemblance to magnetic accretion on to the white dwarf, as previously suggested by Hernanz & Sala (2002). Before speculating on the flare-magnetic accretion link, more spectra with full orbital coverage during flares should be obtained to check, for example, whether the high-velocity emissions are observed at the same orbital phases as reported here.

4.4 Emission from the irradiated companion

Besides the high-velocity emission during the flare, the trailed spectrogram in the vicinity of H α presented in Fig. 5 reveals a narrow emission S-wave in He I $\lambda 6678$ with FWHM ≈ 50 km s $^{-1}$ consistent

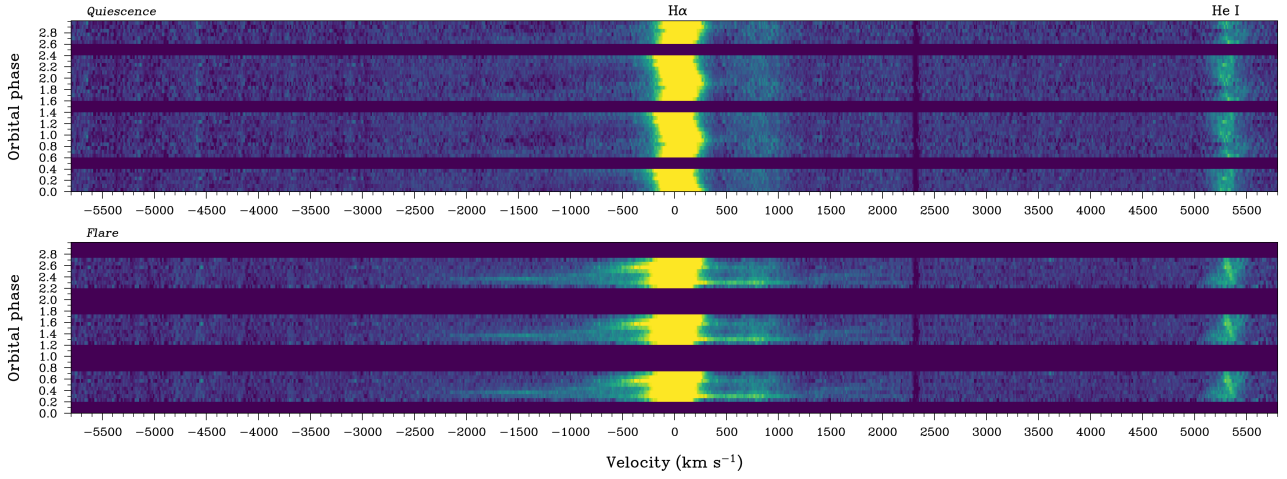


Figure 5. H α and He I λ 6678 trilled spectrograms in quiescence (top; data from the first and third nights) and during a flare (bottom; data from the second night). The spectra have been phase-binned into 15 orbital phase intervals and repeated twice for display purposes. The phase bins with no data are illustrated with dark horizontal stripes.

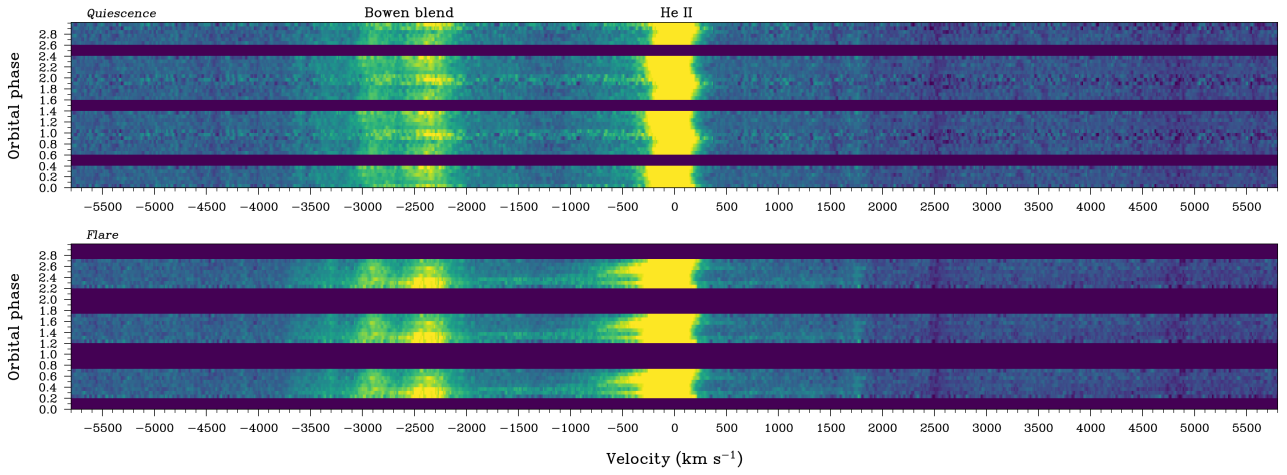


Figure 6. Same as Fig. 5, but for the He II λ 4686 and Bowen blend emissions.

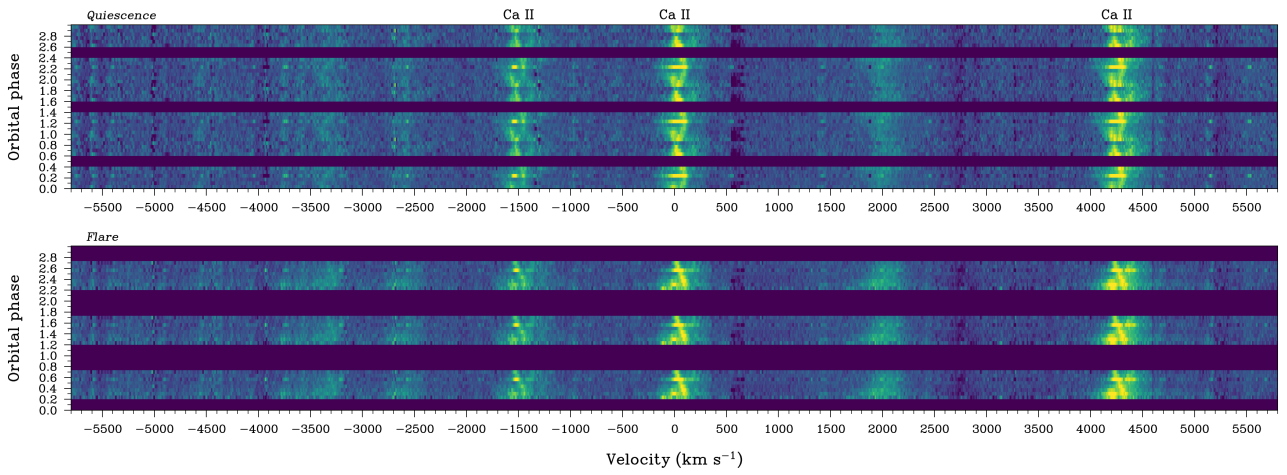


Figure 7. Same as Fig. 5, but for the Ca II emission triplet region.

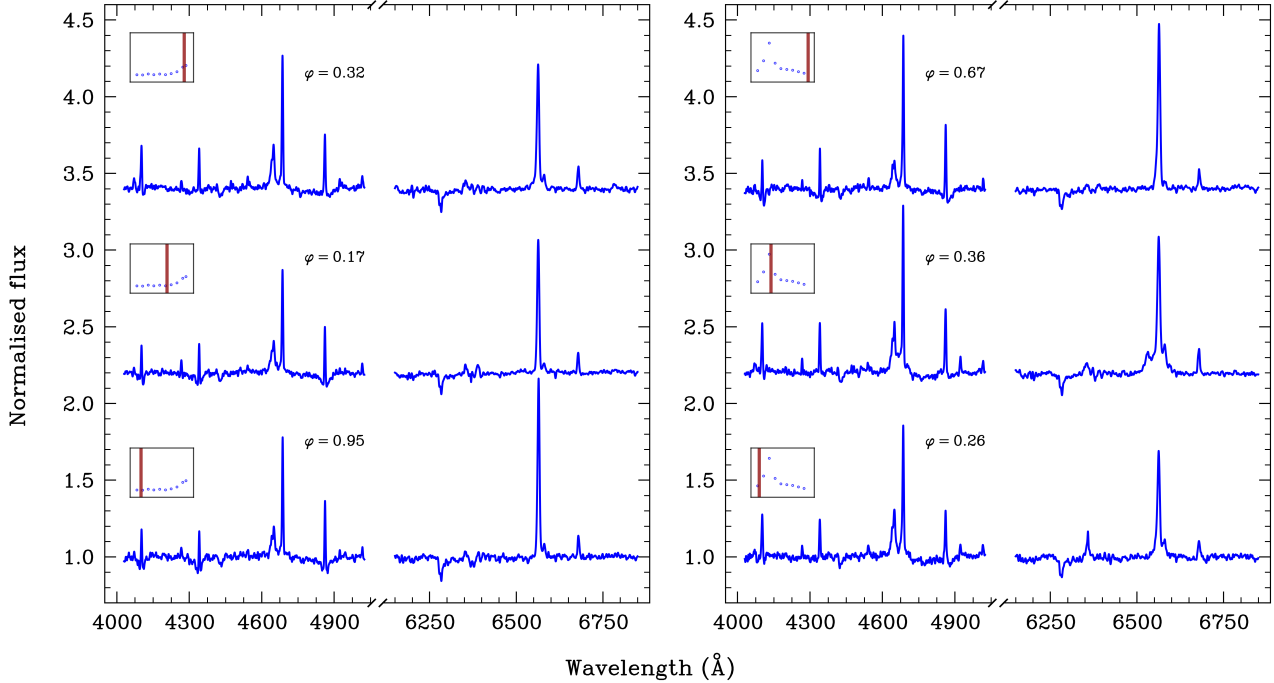


Figure 8. Changes in the spectrum of V2487 Oph with target brightness. The left and right panels correspond to the first and second nights, respectively. The insets show the central time of each spectrum in the light curve presented in Fig. 1. Time runs from bottom to top.

with an origin on the companion star, possibly its heated face. The same emission component is seen in the Ca II triplet during the flare and also in quiescence (Fig. 7), as well as in the O III fluorescence lines and He I (see e.g. the $\lambda 5016$, $\lambda 5876$, and $\lambda 7065$ lines in Fig. A3).

In order to check whether the quiescence and flare spectra can be combined to improve orbital coverage, we used single Gaussian fitting to obtain the radial velocity curve of the Ca II $\lambda 8542$ narrow emission component during the flare (second night spectra only) and of all the spectra combined. The result is illustrated in Fig. 9, and shows that both radial velocity curves are consistent with each other. This way we achieved full-orbit coverage of this line.

Under the assumption that the narrow emission has its origin on the heated face of the companion star, we were able to obtain the time of its inferior conjunction,

$$T_0(\text{HJD}) = 2\,458\,642.6076 \pm 0.019.$$

The phase-binned Ca II $\lambda 8542$ narrow emission and the He II $\lambda 4686$ radial velocity curves are displayed in Fig. 10. If we assume that the Ca II narrow emission is representative of the orbital motion of the companion star, then the He II $\lambda 4686$ radial velocities are delayed by 0.12 cycle relative to the expected motion of the white dwarf, with a maximum blue excursion at phase 0.37. This phase offset is an ubiquitous characteristic of the SW Sex stars and magnetic CVs (e.g. Rodríguez-Gil et al. 2007, 2012; Beuermann et al. 2021). This lends support to our assumption of the Ca II narrow emission having an origin on the hemisphere of the companion star facing the white dwarf, and strengthens the suggestion of Hernanz & Sala (2002) of magnetic accretion.

The radial velocity curves of the O III $\lambda 3133$ and $\lambda 3444$ broad and narrow emissions are also offset relative to each other, as Fig. 11 and Table 2 illustrate, which also points to the companion star as the likely source for the O III fluorescence narrow emission (see also Fig. A1).

In Table 2 we list the parameters of the sine fits to the emission-line

Table 2. Phase-binned radial velocity curve best-fit parameters.

Emission line	γ (km s ⁻¹)	K (km s ⁻¹)	φ_0
Ca II $\lambda 8542$ narrow	63.0 ± 0.6	39.7 ± 0.8	—
He I $\lambda 6678$	50.8 ± 0.7	-32.1 ± 0.9	-0.058 ± 0.005
He II $\lambda 4686$	31.6 ± 0.1	-28.9 ± 0.2	0.116 ± 0.001
H α	34.1 ± 0.1	-33.9 ± 0.2	0.148 ± 0.001
H β	28.6 ± 0.2	-23.1 ± 0.4	0.086 ± 0.002
H γ	39.5 ± 0.4	-20.5 ± 0.6	0.045 ± 0.004
H δ	39.4 ± 0.6	-19.4 ± 0.8	0.015 ± 0.007
O III fluo.	44.6 ± 1.8	-36 ± 3	0.076 ± 0.010
O III $\lambda 3444$ narrow	53 ± 2	25 ± 3	-0.02 ± 0.02
He–H10 absorp. ^{1*}	59.2 ± 0.6	-6.3 ± 0.7	-0.06 ± 0.02

¹ Superimposed emission lines masked out.

* See Section 4.5.

radial velocity curves derived from the phase-binned spectra of the form:

$$V(\varphi) = \gamma + K \sin[2\pi(\varphi - \varphi_0)], \quad (1)$$

with $V(\varphi)$ the radial velocity, γ the systemic velocity, K the radial velocity amplitude, and φ_0 the phase offset. To derive the radial velocities we used cross-correlation with a FWHM = 300 km s⁻¹ Gaussian template except for the narrow emissions, for which we used single Gaussian fitting. Also note that we phase-binned the spectra from the three nights together.

4.5 Radial velocity curve of the accretion disc absorption lines

In Section 3, we showed that the contribution of the white dwarf to the optical flux of V2487 Oph is negligible. Thus, the broad absorption

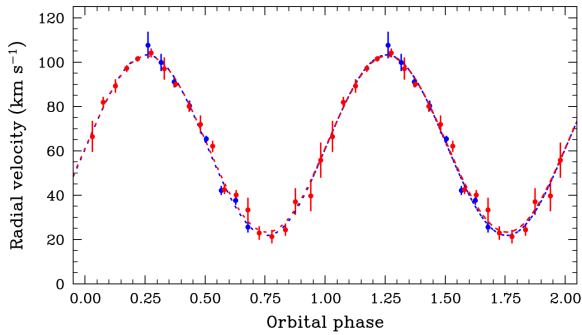


Figure 9. Ca II $\lambda 8542$ narrow emission radial velocity curves of the flare spectra (second night only; blue dots) and of all the spectra combined (red dots). The flare spectra were orbital phase-averaged into 15 bins, and the whole data set into 20 bins prior to measuring the radial velocities by carefully eyeballing the narrow emission component in the trailed spectra and using single Gaussian fitting. The dashed lines are the corresponding best sine fits. A full orbital cycle has been repeated for display purposes.

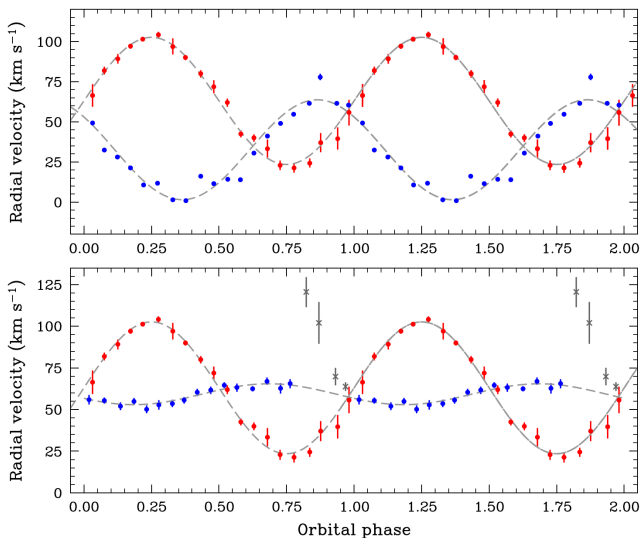


Figure 10. Top panel: Ca II $\lambda 8542$ (red dots) and He II $\lambda 4686$ (blue dots) emission-line radial velocity curves measured from the phase-binned spectra (20 bins). Assuming that the Ca II $\lambda 8542$ narrow emission S-wave follows the motion of the companion star, then He II $\lambda 4686$ is delayed by 0.12 cycle relative to the radial velocity curve expected for the white dwarf. Bottom panel: Phase-binned radial velocity curve through cross-correlation of the He–H10 disc absorption profiles with their average spectrum as the template (blue dots). The emission lines superimposed on the broad absorptions were masked out. The points plotted as grey crosses were excluded from the fitting procedure. The red dots are the same Ca II $\lambda 8542$ narrow emission-line radial velocity curve as the top panel. All data are plotted twice for continuity and the grey dashed lines are the respective best-fit sinusoids.

lines detected in the spectrum are very likely coming from an accretion disc observed at low inclination. To test this, we measured the radial velocities of the Balmer absorption lines by cross-correlation of the He–H10 profiles with their average spectrum as template, after masking the superimposed emission profiles out. The resulting radial velocity curve is presented in the bottom panel of Fig. 10. The phasing, with the minimum and maximum velocity at $\varphi \approx 0.25$ and $\varphi \approx 0.75$, respectively, confirms that the observed absorption lines

likely originate in the accretion disc. In simpler terms, by using the radial velocity curve of the Ca II emission in conjunction with this information, we can make an educated guess about the binary mass ratio of V2487 Oph. The velocity amplitude of the Ca II $\lambda 8542$ narrow emission $K_{\text{em}} = 39.7 \text{ km s}^{-1}$ provides an estimate of the companion star radial velocity amplitude K_2 . On the other hand, let us assume that the amplitude of the He–H10 absorptions radial velocity curve reflects that of the white dwarf, so $K_1 = 6.3 \text{ km s}^{-1}$ (see Table 2). This provides a binary mass ratio $q = M_2/M_1 = K_1/K_2 = 0.16$. Adopting $M_1 = 1.35 M_{\odot}$ (Hachisu et al. 2002), the mass of the companion star would then be $M_2 = 0.21 M_{\odot}$ and its equivalent Roche lobe radius $R_{L2} = 0.96 R_{\odot}$. For a Roche-lobe filling companion star, this might suggest an evolved M-type star in V2487 Oph, possibly a subgiant, considering the orbital period of 18.1 h, as suggested by Darnley et al. (2012). However, the He–H10 absorption lines are contaminated with narrow emission lines from the companion star that can introduce unwanted systematics even if masked to derive their radial velocity curve via cross-correlation with their average profile, not to mention that V2487 Oph is very likely an intermediate polar, so vertical velocity components cannot be neglected. Thus, we deem our assumption that the radial velocity amplitude of these absorptions traces the motion of the white dwarf dubious.

The very hot continuum in V2487 Oph shows the dominance of the accretion flow brightness, as already noted by Schaefer et al. (2022), leaving very little chance of detecting any spectral features of the companion star. However, in order to maximize our chances of detecting any, we eyeballed the trailed spectra diagrams constructed using the quiescence spectra only (15 phase bins; Figs. A4 and A5) to search for absorption lines that may reflect its motion, i.e. radial velocity maxima at orbital phases 0.25 (red) and 0.75 (blue).

We observe candidate absorption lines from the companion star at approximate wavelengths 4148, 4572, 7040, 7480, 7940, 7948, 8088, and 8430 Å, with the last two broader than the rest. There is a strong Fe I line in solar-type stars at 4148 Å, that remains detectable in a wide range of temperature. The possible absorption at 4572 Å could be Ti II. It is present in warmer stars and disappears in late G and K stars. At 7948 Å, a Rb I line is seen in stars with solar temperature or cooler. Note that this is quite speculative and inconsistent in terms of spectral classification, and casts doubts on the tentative donor star mass derived above. However, it hints at the presence of the companion star spectrum and indicates the need for deeper spectra, something feasible for a long orbital period CV such as V2487 Oph while keeping a proper sampling of the binary orbit.

5 CONCLUSIONS

We have measured the orbital period of V2487 Oph to be $0.753 \pm 0.016 \text{ d}$ ($18.1 \pm 0.4 \text{ h}$) from a radial velocity study of its intense He II $\lambda 4686$ emission line. Our value is about 40 per cent shorter than the 1.24 d suggested by the analysis of the K2 light curve presented in Schaefer et al. (2022). We show that no significant power at 0.753 d is present in the periodogram of the whole K2 photometry data set.

We found that the broad Balmer absorption lines seen in quiescence (i.e. out of flare) are produced in the accretion disc. At the distance of V2487 Oph (6.4 kpc), any contribution of the white dwarf to the optical flux can be neglected.

Narrow emissions originating on the heated face of the companion star are observed in the O III fluorescence lines, He II, and the Ca II triplet in the flare spectra. Irradiation may also be present in quiescence.

The trailed spectrograms in quiescence may show absorption lines

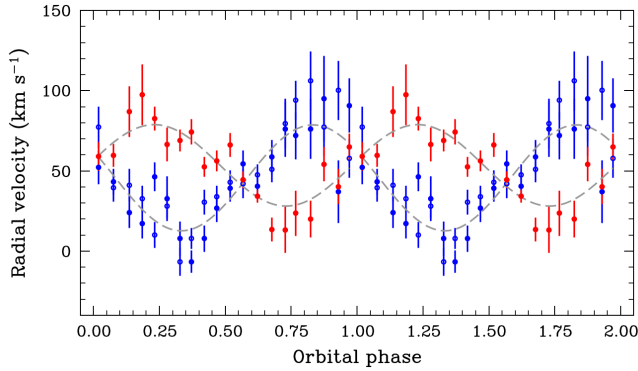


Figure 11. Phase-binned emission-line radial velocity curves of the broader component in O III $\lambda 3133$ (solid blue dots) and $\lambda 3444$ (open blue circles) from cross-correlation with a FWHM = 300 km s⁻¹ Gaussian template. For the narrow emission in O III $\lambda 3444$ (red dots) we used single Gaussian fitting. All data are plotted twice for continuity, and the best-fit sinusoids are superimposed.

from the companion star, but this needs further investigation now that the orbital period of V2487 Oph is known and longer exposure spectra can be taken while still properly sampling the binary orbit.

Analysis of the radial velocity curves resulted in a binary mass ratio $q \approx 0.16$. Assuming a white dwarf mass $M_1 = 1.35 M_\odot$ (Hachisu et al. 2002), a possibly M-type subgiant donor star with mass $M_2 \approx 0.21 M_\odot$ is very tentatively suggested.

The X-shooter spectra from the second night were serendipitously obtained when V2487 Oph was experiencing a flare, during which high-velocity Balmer and He II $\lambda 4686$ emissions exceeding -2000 km s⁻¹ are observed in the blue wings at about $\varphi = 0.4$.

Receding emission is also seen extending up to 1200 km s⁻¹ at $\varphi \approx 0.3$. We suggest that the high-velocity emissions have to do with magnetic accretion on to the white dwarf, as observed in magnetic CVs.

To gain further insight into the spectral changes during the flares relative to quiescence, time-resolved spectroscopy on several nights that provide full orbital coverage should be obtained before the flaring activity in V2487 Oph stops. This would also provide phase-binned spectra in quiescence with a better signal-to-noise ratio to test for absorption lines from the companion star and hopefully reveal its spectral type.

ACKNOWLEDGEMENTS

The authors thank Mike Shara for reviewing the manuscript and for his encouraging report. We also thank Carlos Allende for useful discussion about the candidate absorption features from the companion star. We acknowledge valuable discussion with Brad Schaefer. Based on observations collected at the European Organisation for Astronomical Research in the Southern Hemisphere under ESO programme 103.D-0740(A). PR-G acknowledges support from the Consejería de Economía, Conocimiento y Empleo del Gobierno de Canarias and the European Regional Development Fund (ERDF) under grant with reference ProID2021010132 and ProID2020010104, and also acknowledges support from the ESO Scientific Visitor Programme in Vitacura, Chile. NE-R acknowledges partial support from MIUR, PRIN 2017 (grant 20179ZF5KS), from PRIN-INAF 2022 and from the Spanish MICIN/AEI grant

PID2019-108709GB-I00. This project has received funding from the European Research Council (ERC) under the European Union's Horizon 2020 research and innovation programme (Grant agreement No. 101020057). MH acknowledges funding support from the MICIN/AEI grant PID2019-108709GB-I00, EU-FEDER funds and the AGAUR/Generalitat de Catalunya grant SGR-01526/2021. GS acknowledges funding support from the MICIN/AEI grant PID2020-117252GB-I00, EU-FEDER funds and the AGAUR/Generalitat de Catalunya grant SGR-386/2021. This research was supported in part by the National Science Foundation under Grant No. NSF PHY-1748958.

DATA AVAILABILITY

The data underlying this article will be shared on reasonable request to the corresponding author.

REFERENCES

- Bailer-Jones C. A. L., Rybizki J., Foesneau M., Demleitner M., Andrae R., 2021, *AJ*, **161**, 147
- Beuermann K., Burwitz V., Reinsch K., Schwobe A., Thomas H. C., 2021, *A&A*, **645**, A56
- Bowen I. S., 1934, *PASP*, **46**, 146
- Czesla S., Schröter S., Schneider C. P., Huber K. F., Pfeifer F., Andreasen D. T., Zechmeister M., 2019, PyA: Python astronomy-related packages (ascl:1906.010)
- Darnley M. J., Ribeiro V. A. R. M., Bode M. F., Hounsell R. A., Williams R. P., 2012, *ApJ*, **746**, 61
- Graham M. J., Drake A. J., Djorgovski S. G., Mahabal A. A., Donalek C., 2013, *MNRAS*, **434**, 2629
- Green G. M., Schlafly E., Zucker C., Speagle J. S., Finkbeiner D., 2019, *ApJ*, **887**, 93
- Hachisu I., Kato M., Kato T., Matsumoto K., 2002, in Gänsicke B. T., Beuermann K., Reinsch K., eds, *Astronomical Society of the Pacific Conference Series Vol. 261, The Physics of Cataclysmic Variables and Related Objects*. p. 629 ([arXiv:astro-ph/0110265](https://arxiv.org/abs/astro-ph/0110265))
- Hernanz M., Sala G., 2002, *Science*, **298**, 393
- McClintock J. E., Canizares C. R., Tarter C. B., 1975, *ApJ*, **198**, 641
- Nakano S., Takamizawa K., Kushida R., Kushida Y., Kato T., 1998, *IAU Circ.*, **6941**, 1
- Pagnotta A., Schaefer B. E., Xiao L., Collazzi A. C., Kroll P., 2009, *AJ*, **138**, 1230
- Raymond J. C., Black J. H., Davis R. J., Dupree A. K., Gursky H., Hartmann L., Matilsky T. A., 1979, *ApJ*, **230**, L95
- Rodríguez-Gil P., et al., 2007, *MNRAS*, **377**, 1747
- Rodríguez-Gil P., Schmidtbreick L., Long K. S., Gänsicke B. T., Torres M. A. P., Rubio-Díez M. M., Santander-García M., 2012, *MNRAS*, **422**, 2332
- Schachter J., Filippenko A. V., Kahn S. M., Paerels F. B. S., 1991, *ApJ*, **373**, 633
- Schaefer B. E., 2010, *ApJS*, **187**, 275
- Schaefer B. E., Pagnotta A., Zoppelt S., 2022, *MNRAS*, **512**, 1924
- Shrader C. R., Singh K. P., Barrett P., 1997, *ApJ*, **486**, 1006
- Vernet J., et al., 2011, *A&A*, **536**, A105
- Zechmeister M., Kürster M., 2009, *A&A*, **496**, 577

APPENDIX A: TRAILED SPECTRA PLOTS

Figs. A1 to A3 illustrate the trailed spectrograms using all the spectra (quiescence and flare state) phase-binned into 20 bins, while the trailed spectra plots presented in Figs. A4 to A5 were constructed

using the quiescence spectra only (first and third night) after applying a 15-bin phase binning.

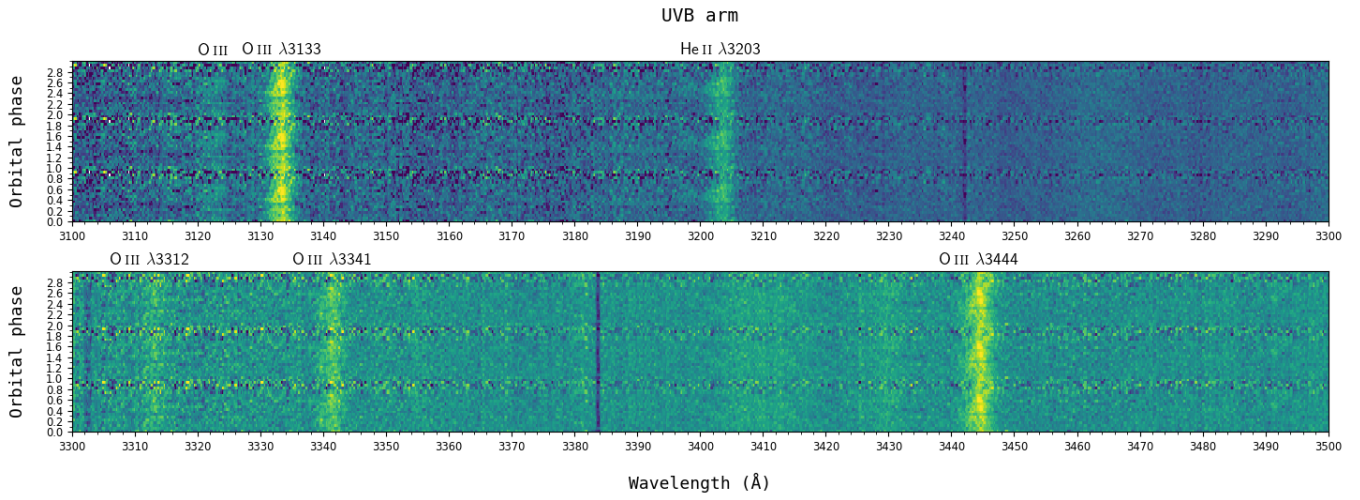


Figure A1. Trailed spectra diagrams in the far blue fluorescence emission line region after averaging all the spectra into 20 phase bins. The orbital cycle is repeated twice. The two most intense O III emission lines are labelled.

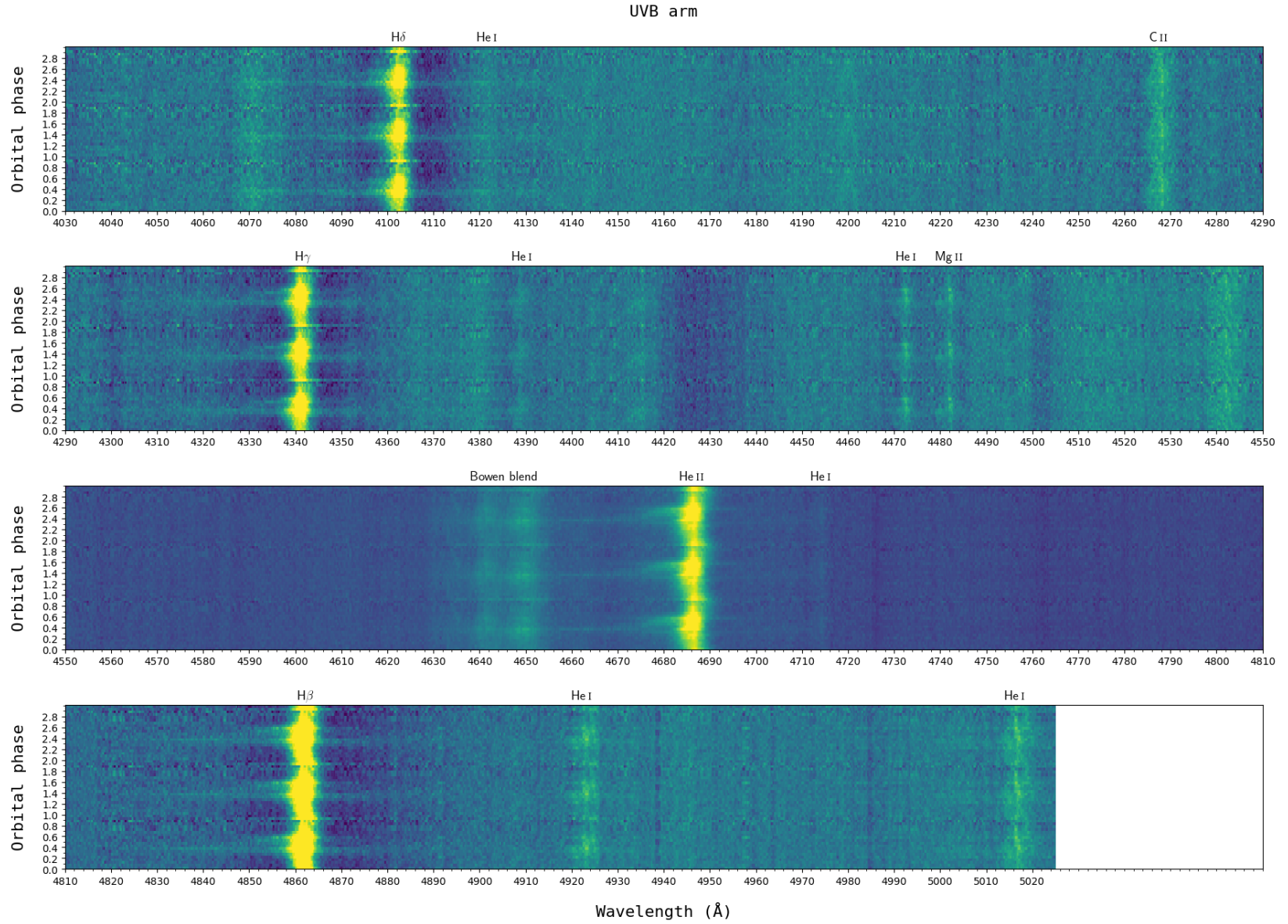


Figure A2. X-shooter UVB arm trailed spectra diagrams using all the data averaged into 20 orbital phase bins. The full cycle has been repeated twice for clarity.

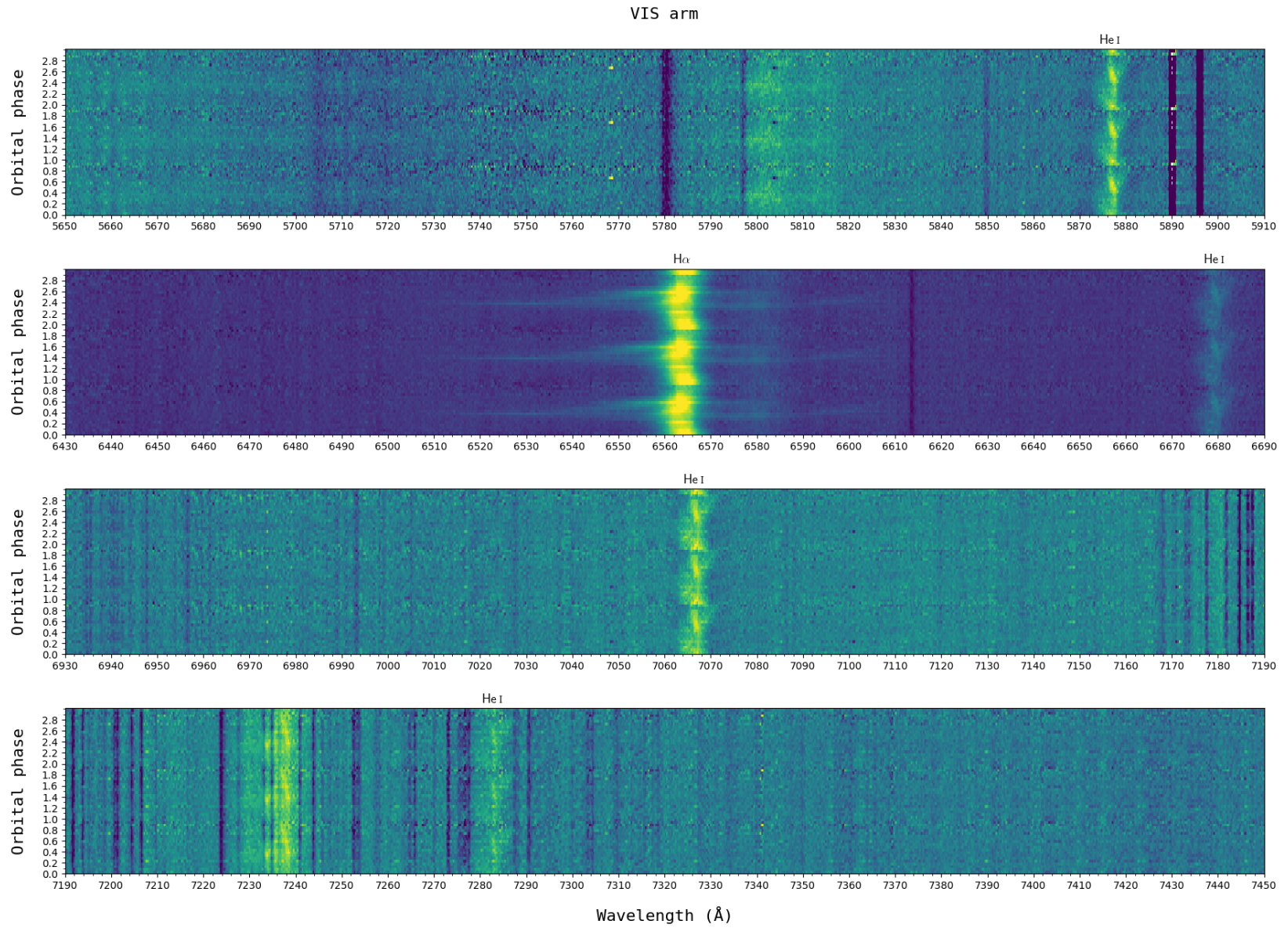


Figure A3. Same as Fig. A2, but for the VIS arm.

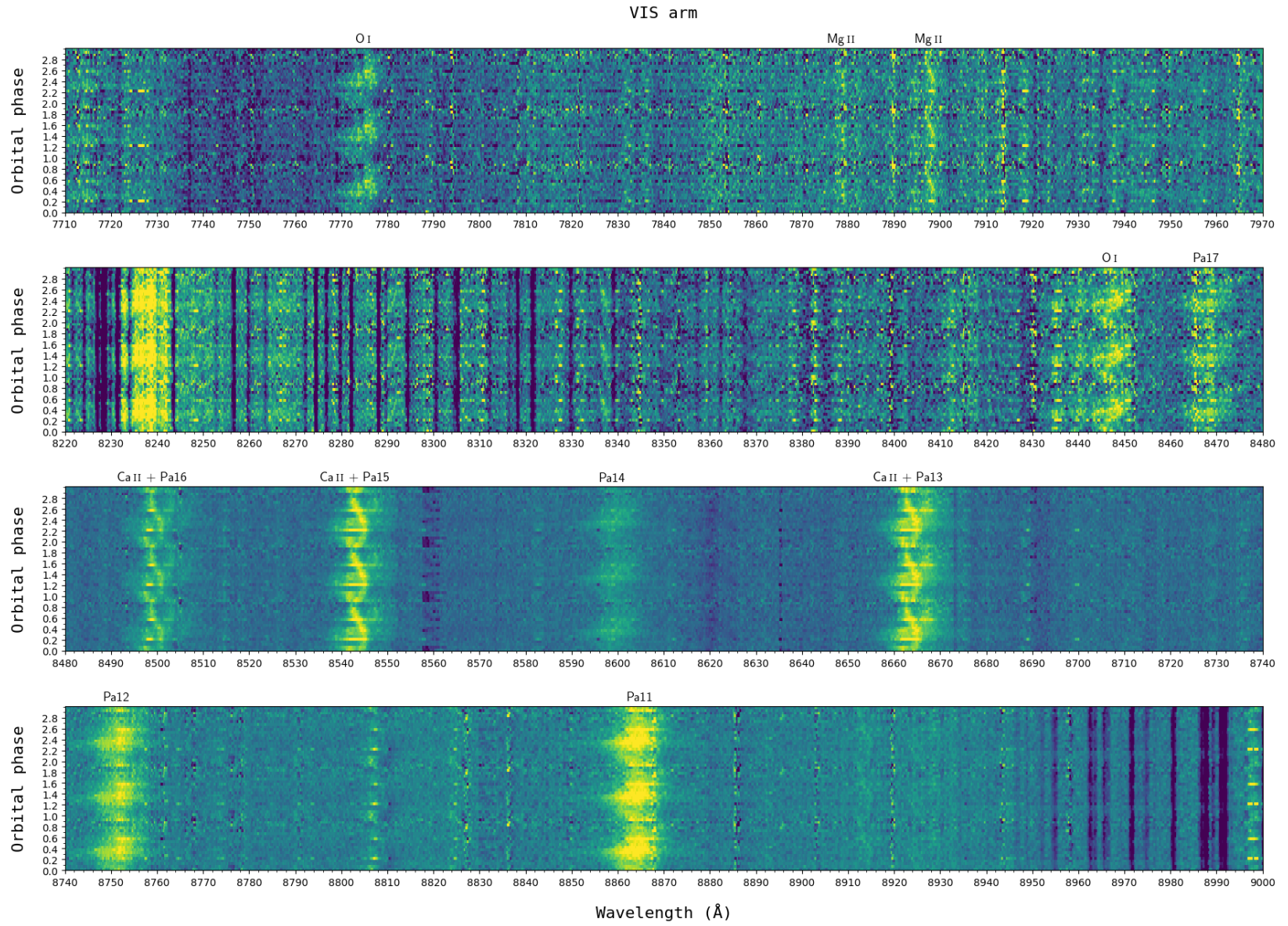


Figure A3 (cont.).

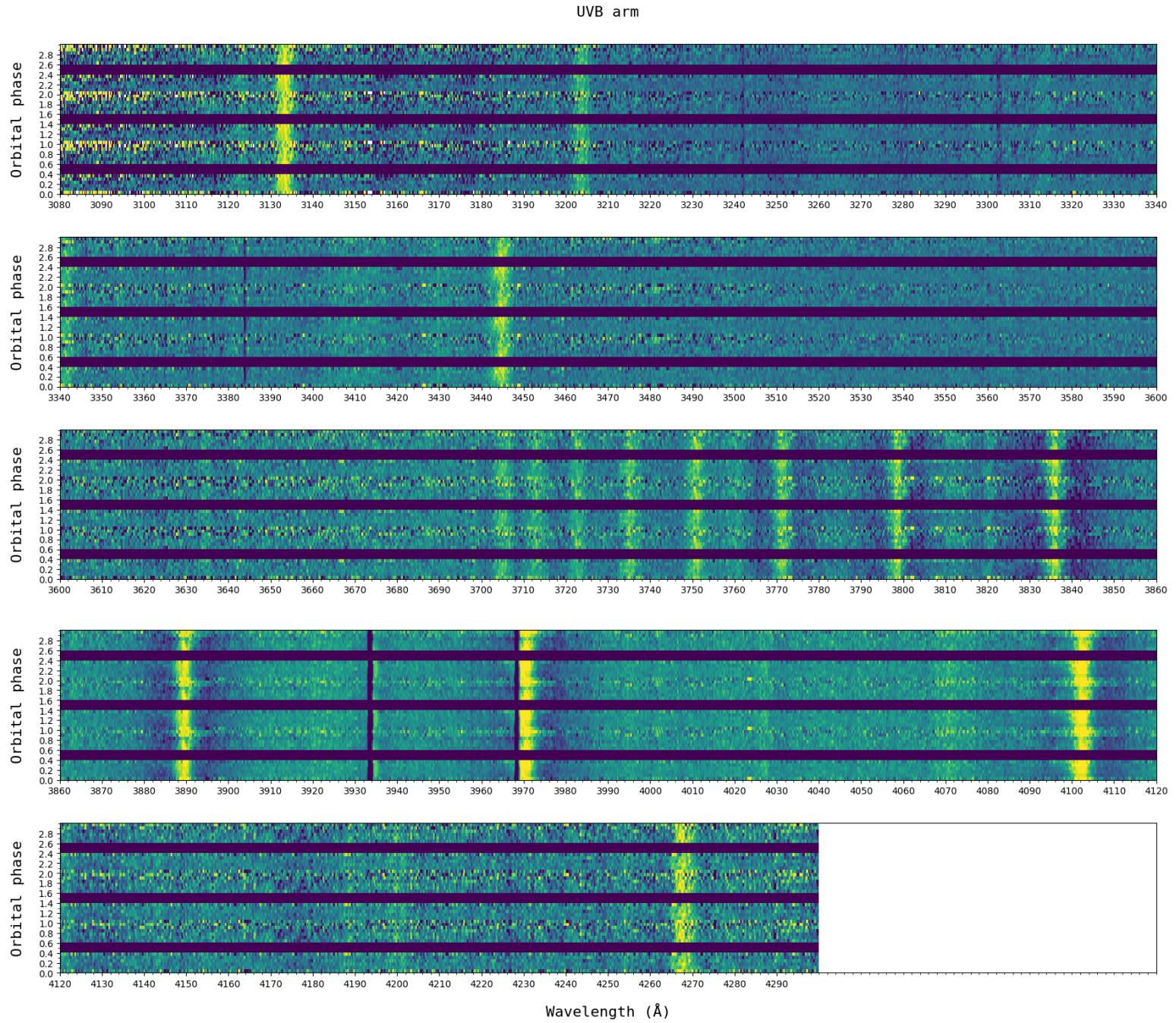


Figure A4. X-shooter UVB arm trailed spectra diagrams using only the data in quiescence averaged into 15 orbital phase bins. The full cycle has been repeated twice for clarity.

UVB arm

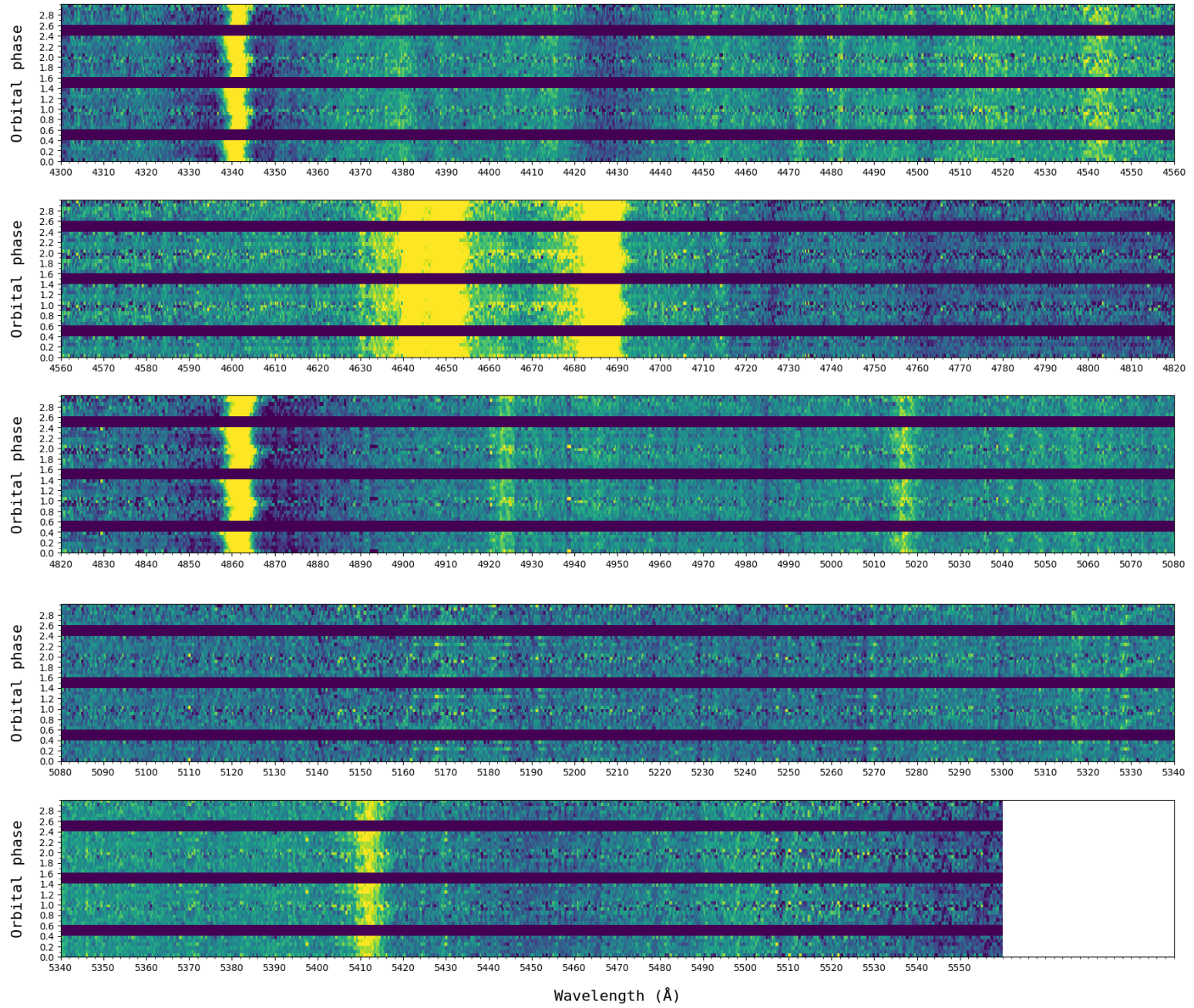


Figure A4 (cont.).

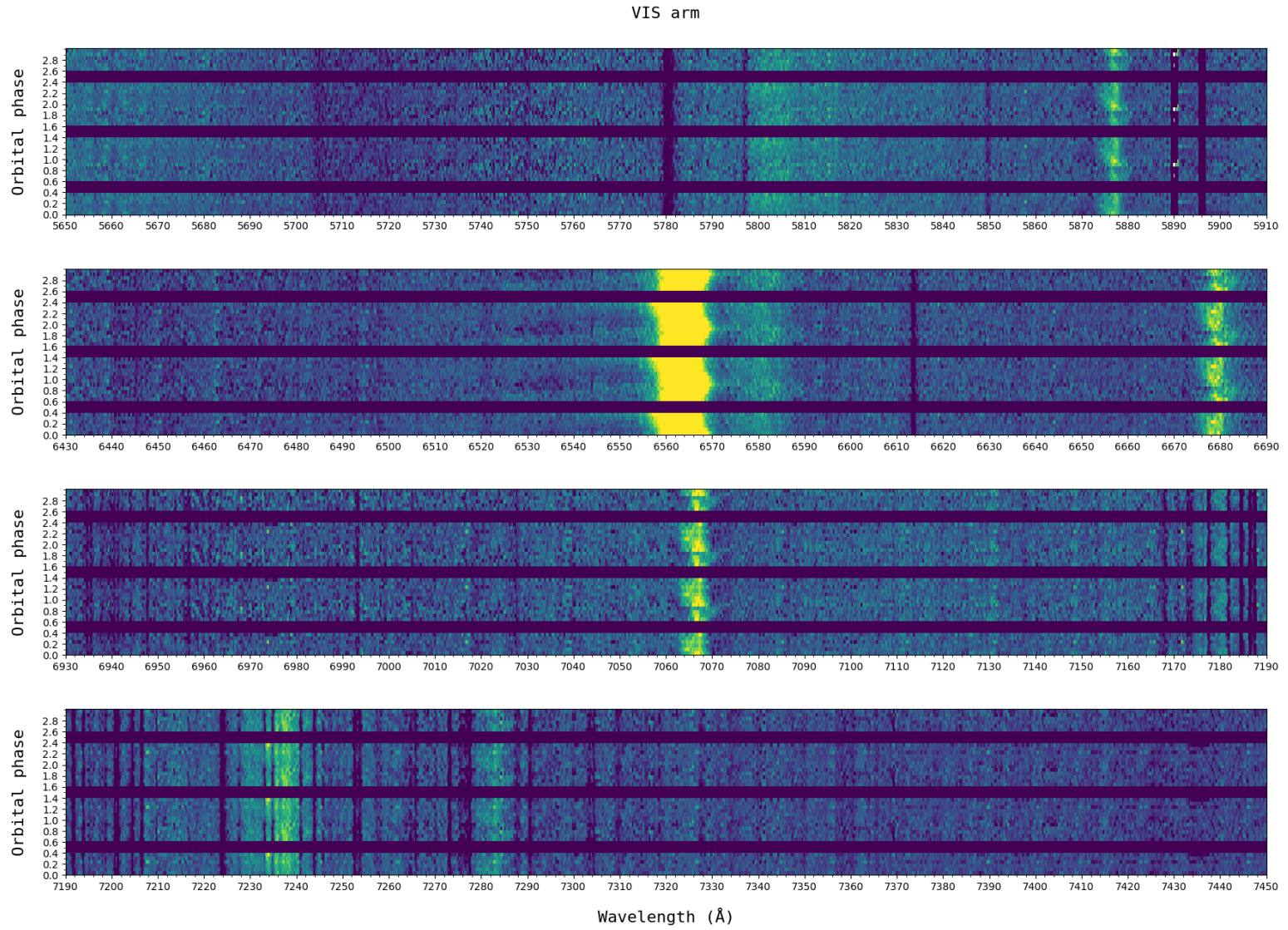


Figure A5. Same as Fig. A4, but for the VIS arm.

VIS arm

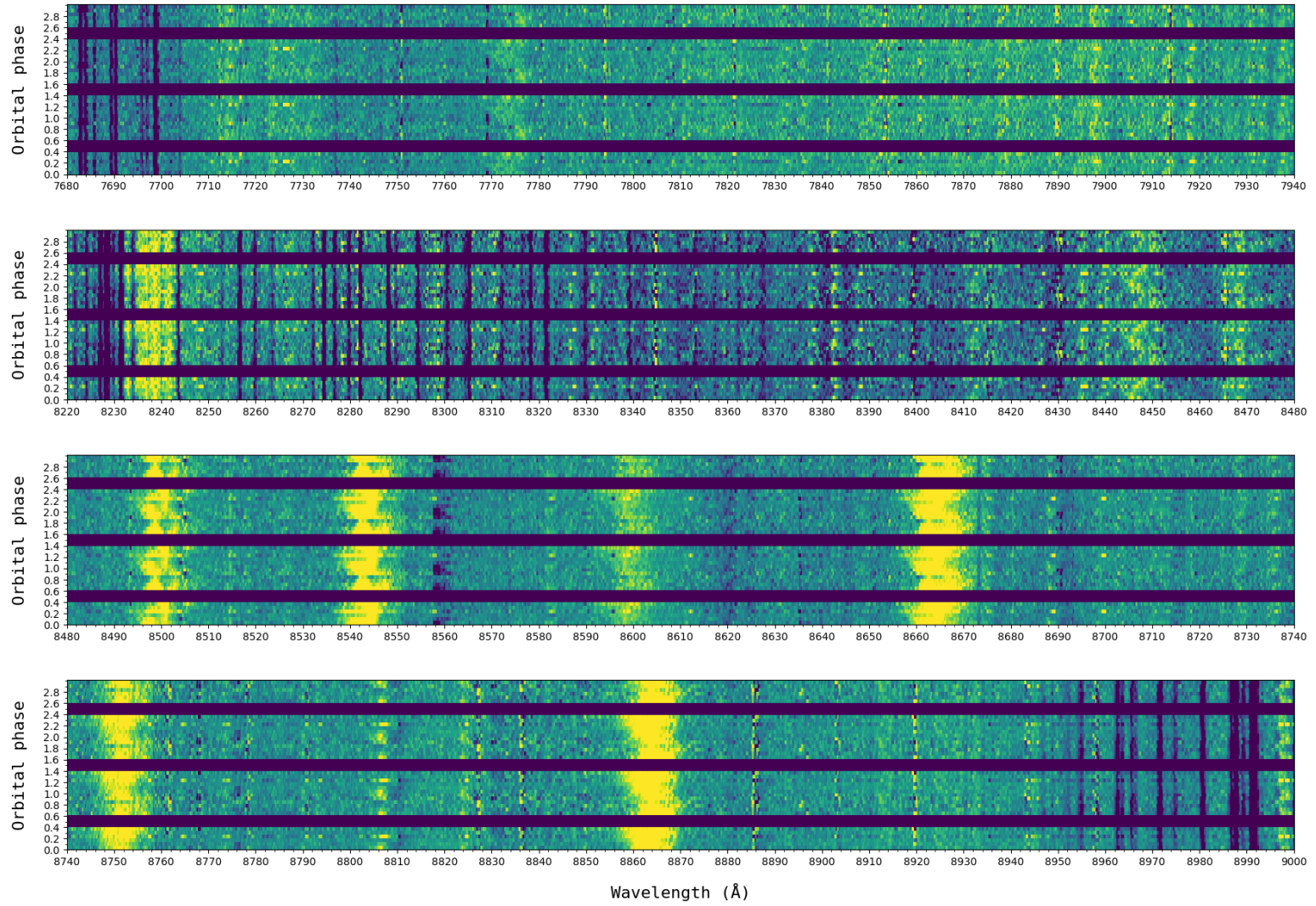


Figure A5 (cont.).

This paper has been typeset from a \TeX/L\AA\TeX file prepared by the author.